Demura, M.					
Yoshida, K.; Yamamoto, K.; Kohno, T.; Hironaka, N.; Yasui, K.; Kojima, C.; Mukae, H.; Kadota, J.; Suzuki, S.; Honma, K.; Kohno, S.; Matsuyama, T.	Active Repression of IFN Regulatory Factor-1-Mediated Transactivation by IFN Regulatory Factor-4	*Int. Immunol.*	*17*	1463-1471	2005
Nakatani, K.; Hagihara, S.; Goto, Y.; Kobori, A.; Hagihara, M.; Hayashi, G.; Kyo, M.; Nomura, M.; Mishima, M.; Kojima, C.	Solution structure of a small-molecule ligand complexed with CAG trinucleotide repeat DNA	*Nucleic Acids Res. Suppl.*	*5*	49-50	2005
Tanaka, Y.; Yamaguchi, H.; Oda, S.; Kojima, C.; Ono, A.; Taira, K.; Kondo, Y.	NMR spectroscopic analyses of functional nucleic acids-metal interaction and their solution structure analyses	*Nucleic Acids Res. Suppl.*	*5*	51-52	2005
Yamaguchi, H.; Oda, S.; Kojima, C.; Ono, A.; Kondo, Y.; Tanaka, Y.	Spectroscopic analyses of DNA duplexes in the presence of mercury ions	*Nucleic Acids Res. Suppl.*	*5*	199-200	2005
NMR structural analysis of the G.G Mismatch DNA	NMR structural analysis of the G.G Mismatch DNA complexed with	*Nucleic Acids Res. Suppl.*	*5*	213-214	2005

complexed with Naphthyridine-Dimer, Nomura, M.; Hagihara, S.; Goto, Y.; Nakatani, K.; Kojima, C.	Naphthyridine-Dimer				

研究成果の刊行物・別刷

Available online at www.sciencedirect.com
SCIENCE DIRECT®
Bioorganic & Medicinal Chemistry Letters
ELSEVIER
Bioorganic & Medicinal Chemistry Letters 15 (2005) 259–262

A new ligand binding to G–G mismatch having improved thermal and alkaline stability

Tao Peng,[b] Takashi Murase,[a] Yuki Goto,[a] Akio Kobori[b] and Kazuhiko Nakatani[a,b,*]

[a]*Department of Synthetic Chemistry and Biological Chemistry, Faculty of Engineering, Kyoto University, Kyoto 606-8501, Japan*
[b]*PRESTO, Japan Science and Technology Agency (JST), Kyoto 615-8510, Japan*

Received 4 October 2004; revised 28 October 2004; accepted 30 October 2004
Available online 21 November 2004

Abstract—Naphthyridine dimer (**ND**) specially binds to guanine–guanine (G–G) mismatch in duplex DNA. In order to improve the thermal and alkaline stability and binding ability of the ligand, we have examined structural modification of the linker. A new ligand (**NNC**) possessing 2-amino-1,8-naphthyridines and a carbamate linker is much more thermally stable than **ND**. The half-life of **NNC** is 2.5 times longer than that of **ND** at 80 °C. **NNC** is also much more stable than **ND** under alkaline conditions. In addition, **NNC** binds to G–G mismatch more strongly than **ND**. The improved stability and the binding of **NNC** to the G–G mismatch would be suitable for the practical use of **NNC**-immobilized sensor.

Since a draft sequence of the human genome was determined,[1,2] some 1.6 million human single nucleotide polymorphisms (SNPs) have been found in the human genome and deposited to public databases.[3] SNPs became extremely important as a genetic marker for the identification of disease genes and detection of genetic mutations.[4,5] Thus, simple and rapid detection of a single nucleotide difference in the DNA sequences is an indispensable technique for both SNP mapping and typing. Although a number of methods have been developed for SNPs typing,[4,6,7] there is still a great need for designing new typing methods that are simple in operation, rapid and accurate in analysis, and low in cost.

We have recently reported a novel approach for the detection of SNPs by sensing guanine–guanine (G–G) mismatches in duplex DNA.[8] We have developed a sensor chip that can detect G–G mismatches in duplex DNA by means of surface plasmon resonance (SPR).[9,10] The sensor was prepared by immobilizing mismatch binding ligand naphthyridine dimer (**ND**) onto the carboxylated dextran matrix on the gold surface. We have reported that **ND** binds selectively to G–G mismatches in duplex DNA.[8,11] During the regeneration process of the **ND**-immobilized surface under alkaline conditions after each mismatch analysis, it was observed that the immobilized **ND** was slowly degraded under the conditions. We also found that high temperature necessary for denaturing the bound duplex on **ND**-immobilized sensor induced the **ND** degradation. Improving the thermal and alkaline stability of the mismatch-binding ligand eventually leads to a prolonged sensor lifetime. We report here a novel G–G mismatch binding ligand (**NNC**) that has not only greatly improved thermal and alkaline stability but also the higher affinity and selectivity to the G–G mismatch compared to **ND** (Fig. 1).

To gain insights into the degradation pathway, we first examined the thermal reaction of **ND** at 80 °C in 100 mM sodium cacodylate (pH 7.0) by HPLC (Fig. 2).

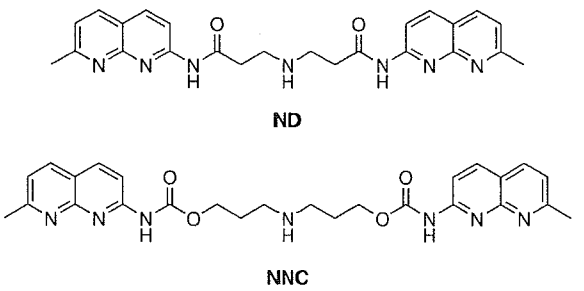

Figure 1. **ND** and **NNC**.

Keywords: DNA; Recognition; Mismatch.
* Corresponding author. Tel.: +81 753832756; fax: +81 753832759; e-mail: nakatani@sbchem.kyoto-u.ac.jp

0960-894X/$ - see front matter © 2004 Elsevier Ltd. All rights reserved.
doi:10.1016/j.bmcl.2004.11.003

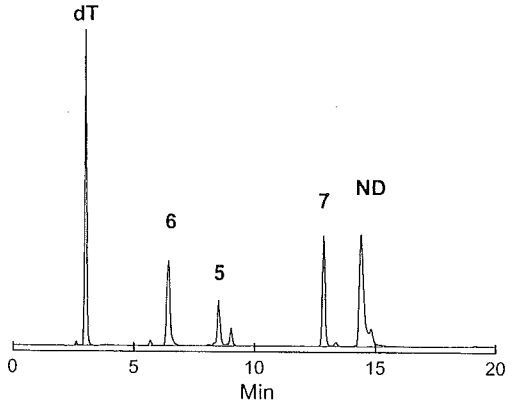

Figure 2. HPLC profile for the thermolysis of **ND** (0.71 mM) in 100 mM sodium cacodylate buffer (pH 7.0) for 45 min at 80 °C. dT was added as an internal standard.

The dT was selected as an internal standard for the thermolysis so that the reproducible and quantitative data could be obtained from the chromatographs. We detected three major products, which were identified as 2-amino-7-methyl-1,8-naphthyridine (**5**), 3-amino-*N*-(7-methyl-1,8-naphthyridin-2-yl)-propionamide (**6**), and *N*-(7-methyl-1,8-naphthyridin-2-yl)-acrylamide (**7**). The formation of **5** suggested the hydrolysis of the amide linkage, where as β-elimination was another degradation pathway producing **6** and **7** (Fig. 3).

To suppress both degradation processes and retain the binding ability to the G–G mismatch, a new molecule **NNC**, where amide linkage was substituted by a carbamate linkage, was synthesized. In addition, the alkyl chain length was further extended by one carbon for each side to slow down the nucleophilic addition of the secondary amino group in the linker to the carbonyl group leading to a release of **5**.

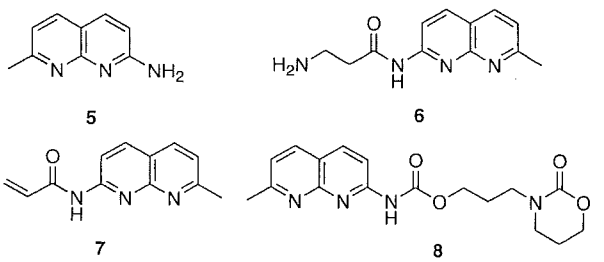

Figure 3. The products derived from thermolysis of **ND** and **NNC**.

NNC was synthesized as shown in Scheme 1. *N*-Boc-dipropanolamine was reacted with *N*,*N*′-disuccinimidyl carbonate (DSC) in dry acetonitrile to produce carbonate,[12] which was then reacted with 2-amino-7-methyl-1,8-naphthyridine to afford Boc-protected **NNC**. Deprotection by hydrogen chloride in ethyl acetate gave hydrochloride salt of **NNC**.[13]

The thermal reaction of **NNC** was examined under the same condition as that of **ND** (Fig. 4).

The major products of the **NNC** degradation after incubating at 80 °C for 120 min were identified as **5** and (7-methyl-1,8-naphthyridin-2-yl)-carbamic acid 3-(2-oxo-1,3-oxazinan-3-yl)-propyl ester (**8**) (Fig. 3). After a periodic incubation, the amount of **ND** and **NNC** were analyzed by HPLC. The rate of thermolysis could be determined from the decrease of the ligands. The half-life curves for the thermolysis of **NNC** and **ND** were shown in Figure 5. It is clearly shown that the half-life of **ND** is about 40 min at 80 °C, whereas the half-life of

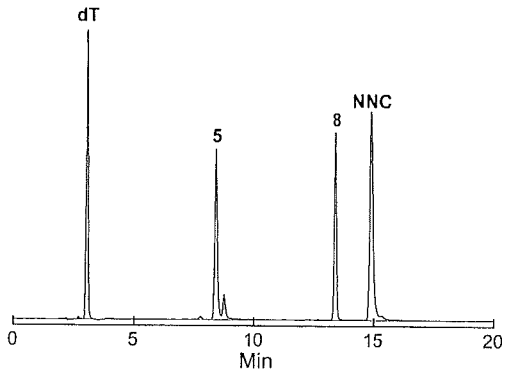

Figure 4. HPLC profile for the thermolysis of **NNC** (0.71 mM) in 100 mM sodium cacodylate buffer (pH 7.0) for 120 min at 80 °C.

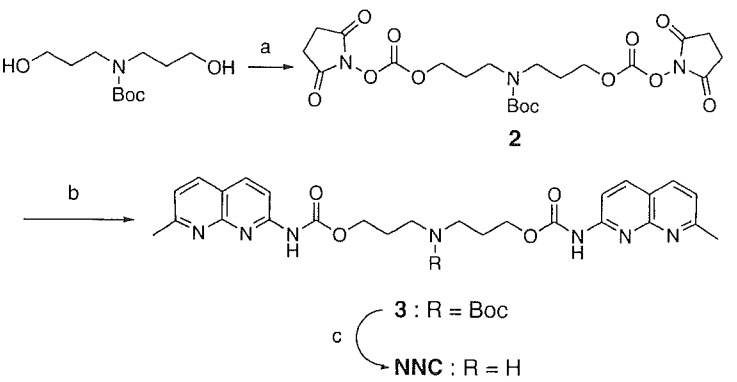

Scheme 1. Reagents and conditions: (a) *N*,*N*′-disuccinimidyl carbonate, CH_3CN, Et_3N; (b) 2-amino-7-methyl-1,8-naphthyridine, CH_2Cl_2, Et_3N, 49% for two steps; (c) HCl, AcOEt, $CHCl_3$, quantitative.

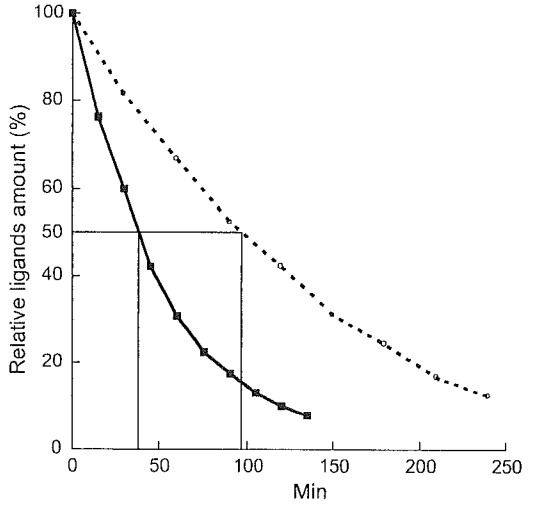

Figure 5. The half-life curves of **ND** (—) and **NNC** (···) in 100 mM sodium cacodylate buffer (pH 7.0) at 80 °C. *Y*-Axis represents the relative amount of ligands remained after incubation.

NNC is about 100 min. These results showed that the ligand **NNC** is much more thermally stable than **ND**.

The stabilities of the ligands in alkaline conditions were also examined incubating at room temperature in 50 mM sodium hydroxide (Fig. 6). Under the alkaline conditions, only 29% of **ND** remained after 2 h incubation, whereas 86% of **NNC** still remained under the same conditions. After incubation for 4 h, the amount of **ND** and **NNC** remaining was 7% and 79%, respectively. It is very clear that **NNC** is much more stable than **ND** in an alkaline solution.

Having confirmed the improved stability of **NNC** under the thermal and alkaline conditions, we then looked at

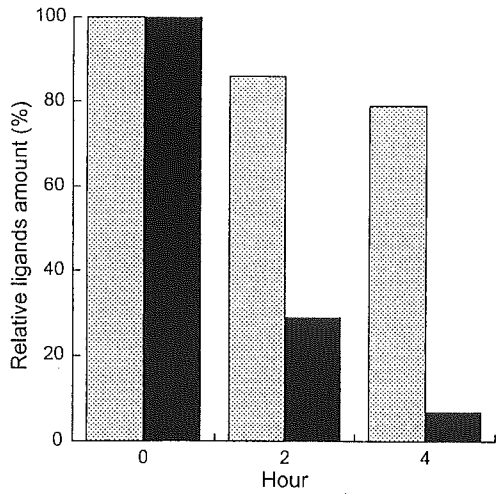

Figure 6. The amount of **ND** (solid bar) and **NNC** (shaded bar) (100 μM) remaining after incubation in 50 mM sodium hydroxide and 100 mM sodium chloride at room temperature. The amount was obtained by HPLC relative to the dT added as an internal standard. *Y*-Axis represents the relative amount of ligands remaining after incubation.

Table 1. ΔT_m of mismatch-containing duplexes in the presence ligands[a]

X–*Y*	T_m	ΔT_m[b]	
		NNC	ND
A–A	17.8 (1.4)	1.5 (0.2)	−0.8 (1.1)
A–C	16.1 (0.8)	4.1 (0.2)	2.1 (0.2)
C–C	18.2 (0.2)	6.1 (0.3)	6.7 (0.6)
G–A	25.7 (0.2)	7.0 (0.2)	8.6 (1.3)
G–G	25.6 (1.3)	29.1 (0.2)	23.7 (1.2)
G–T	28.3 (0.2)	1.2 (0.8)	10.2 (1.3)
T–C	18.6 (0.2)	3.7 (0.3)	5.5 (0.7)
T–T	25.1 (0.2)	0.7 (0.7)	0.6 (1.2)
A–T	34.3 (0.3)	0.0 (0.3)	−1.5 (0.3)
G–C	40.3 (0.0)	−2.0 (0.4)	2.0 (0.9)

[a] The UV-melting curve was measured for a duplex of d(CTA AC*X* GAA TG)/d(CAT TC*Y* GTT AG) at a total base concentration of 100 μM in a 10 mM sodium cacodylate buffer (pH 7.0) containing 0.1 M NaCl. A mismatch (*X*–*Y*) is produced in the middle of the duplex. Temperature was increased at a rate of 1 °C/min. All measurements were taken three times, and standard deviations are shown in the parentheses.

[b] ΔT_m is calculated as a difference of T_m in the presence and absence of drugs (100 μM), respectively.

the selective binding of **NNC** to the G–G mismatch. The assay was carried out by measuring the melting temperature (T_m) of 11-mer duplexes d(CTA AC*X* GAA TG)/d(CAT TC*Y* GTT AG) (where *X*, *Y* = A, G, T, or C) containing mismatches in the absence and presence of **NNC** (Table 1). T_m increase (ΔT_m) of the duplex containing a G–G mismatch was 23.7 °C in the presence of **ND** (100 μM). Under identical conditions, ΔT_m of 29.1 °C was recorded in the presence of **NNC**. The difference of ΔT_m ($\Delta\Delta T_m$) between **NNC** and **ND** for the G–G mismatch was 5.4 °C, suggesting that the modification of the linker structure of **ND** to that of **NNC** has a positive effect for the thermodynamic stabilization of the G–G mismatch by **NNC**. This is most likely due to an expanded π-surface in a carbamate linkage and a release of the linker strain involved in the bound DNA–**ND** complex. The affinity of **NNC** to the G–G mismatch was calculated by the curve fitting of the UV-melting curve obtained in the absence and presence of **NNC** to the theoretical equation.[14] The K_a obtained for the assumed 1:1 binding between **NNC** to the G–G mismatch was $>10^7 M^{-1}$, that is larger than the K_a we reported for the **ND** binding to the G–G mismatch.

All of the data presented here showed that the ligand **NNC** is a better ligand than **ND** in terms of the affinity and selectivity to the G–G mismatch, and the thermal and alkaline stability. The use of **NNC** for the SPR sensor would enhance the sensitivity to the G–G mismatch by eliminating the unnecessary binding to DNA containing other mismatches. Furthermore, with a higher thermal and alkaline stability, **NNC** can be applied more expansively than **ND**.

References and notes

1. Lander, E. S. et al. *Nature* **2001**, *409*, 860–921.
2. Venter, C. J. et al. *Science* **2001**, *291*, 1304–1351.

3. http://www.ncbi.nlm.nih.gov/SNP/.
4. Schafer, A. J.; Hawkins, J. R. *Nat. Biotechnol.* **1998**, *16*, 33–39.
5. Collins, F. S.; Guyer, M. S.; Chakravarti, A. *Science* **1997**, *278*, 1580–1581.
6. SyvaÈnen, A. C. *Nature Rev. Genet.* **2001**, *2*, 930–942.
7. Kwok, P. Y. *Annu. Rev. Genom. Hum. Genet.* **2001**, *2*, 235–258.
8. Nakatani, K.; Sando, S.; Saito, I. *Nat. Biotechnol.* **2001**, *19*, 51–55.
9. Nice, E. C.; Catimel, B. *Bioessays* **1999**, *21*, 339–352.
10. Fivash, M.; Towler, E. M.; Fisher, R. *Curr. Opin. Biotechnol.* **1998**, *9*, 97–101.
11. Nakatani, K.; Sando, S.; Kumasawa, H.; Kikuchi, J.; Saito, I. *J. Am. Chem. Soc.* **2001**, *123*, 12650–12657.
12. Ghosh, A. K.; Duong, T. T.; McKee, S. P.; Thompson, W. J. *Tetrahedron Lett.* **1992**, *33*, 2781–2784.
13. The data of the hydrochloride salt of **NNC**: ^{1}H NMR (CD_3OD, 400 MHz): $\delta = 8.15$ (m, 6H), 7.35 (d, 2H, $J = 8.4$ Hz), 4.34 (t, 4H, $J = 6.0$ Hz), 3.15 (t, 4H, $J = 7.2$ Hz), 2.71 (s, 6H), 2.11 (br s, 4H). ^{13}C NMR (CD_3OD, 400 MHz): $\delta = 163.0$, 154.5, 154.3, 154.0, 139.1, 137.6, 121.4, 118.2, 113.1, 62.7, 45.4, 26.5, 23.8. HR-FABMS calcd for $C_{26}H_{30}N_7O_6$ [$(M+H)^+$], 504.2359. Found: 504.2361.
14. Nakatani, K.; Horie, S.; Murase, T.; Hagihara, S.; Saito, I. *Bioorg. Med. Chem.* **2003**, *11*, 2347–2353.

nature
chemical biology

Small-molecule ligand induces nucleotide flipping in $(CAG)_n$ trinucleotide repeats

Kazuhiko Nakatani[1,2,5], Shinya Hagihara[1], Yuki Goto[1], Akio Kobori[2], Masaki Hagihara[2,5], Gosuke Hayashi[1], Motoki Kyo[3], Makoto Nomura[4], Masaki Mishima[4] & Chojiro Kojima[4]

DNA trinucleotide repeats, particularly CXG, are common within the human genome. However, expansion of trinucleotide repeats is associated with a number of disorders, including Huntington disease, spinobulbar muscular atrophy and spinocerebellar ataxia[1–4]. In these cases, the repeat length is known to correlate with decreased age of onset and disease severity[5,6]. Repeat expansion of $(CAG)_n$, $(CTG)_n$ and $(CGG)_n$ trinucleotides may be related to the increased stability of alternative DNA hairpin structures consisting of CXG-CXG triads with X-X mismatches[7–11]. Small-molecule ligands that selectively bound to CAG repeats could provide an important probe for determining repeat length and an important tool for investigating the *in vivo* repeat extension mechanism. Here we report that napthyridine-azaquinolone (NA, 1) is a ligand for CAG repeats and can be used as a diagnostic tool for determining repeat length. We show by NMR spectroscopy that binding of NA to CAG repeats induces the extrusion of a cytidine nucleotide from the DNA helix.

The expansion of $(CAG)_n$ trinucleotide repeats in genomic DNA is related to the pathogenesis of Huntington disease, the spinobulbar muscular atrophy known as Kennedy disease, and spinocerebellar ataxia. The $(CAG)_n$ repeat in normal IT15 genes ranges from 6 to 39 trinucleotide repeats, but the trinucleotide is repeated up to 121 times in patients with Huntington disease[3]. Although the mechanism of repeat expansion remains unclear, it is believed to involve strand slippage during DNA synthesis mediated by the formation of an alternative DNA hairpin structure. Because the stability of the hairpin

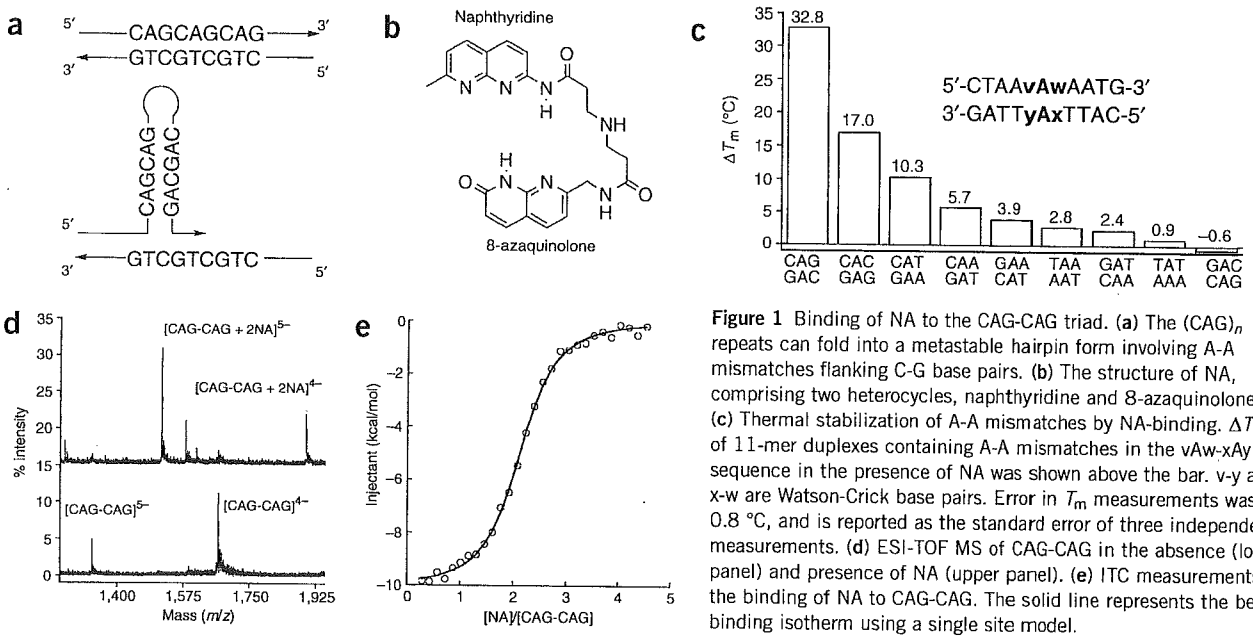

Figure 1 Binding of NA to the CAG-CAG triad. (**a**) The $(CAG)_n$ repeats can fold into a metastable hairpin form involving A-A mismatches flanking C-G base pairs. (**b**) The structure of NA, comprising two heterocycles, naphthyridine and 8-azaquinolone. (**c**) Thermal stabilization of A-A mismatches by NA-binding. ΔT_m of 11-mer duplexes containing A-A mismatches in the vAw-xAy sequence in the presence of NA was shown above the bar. v-y and x-w are Watson-Crick base pairs. Error in T_m measurements was ± 0.8 °C, and is reported as the standard error of three independent measurements. (**d**) ESI-TOF MS of CAG-CAG in the absence (lower panel) and presence of NA (upper panel). (**e**) ITC measurements for the binding of NA to CAG-CAG. The solid line represents the best-fit binding isotherm using a single site model.

[1]Department of Synthetic Chemistry and Biological Chemistry, Graduate School of Engineering, Kyoto University, Kyoto 615-8510, Japan. [2]PRESTO, Japan Science and Technology Agency, 4-1-8 Honcho Kawaguchi, Saitama 332-0012, Japan. [3]Biotechnology Frontier Project, TOYOBO Co. Ltd., Tsuruga, Fukui 914-0047, Japan. [4]Graduate School of Biological Science, Nara Institute of Science and Technology, Nara 630-0101, Japan. [5]Present address: The Institute of Scientific and Industrial Research (SANKEN), Osaka University, 8-1 Mihogaoka, Ibaraki 567-0047, Japan. Correspondence should be addressed to K.N. (nakatani@sanken.osaka-u.ac.jp) or C.K. (kojima@bs.naist.jp).

Published online 24 May 2005; doi:10.1038/nchembio708

form increases as the repeat expands, the repeat length is one of the most important determinants for diagnosis of disease severity and investigations of the expansion mechanism. The hairpin form of $(CAG)_n$ repeats involves the intramolecular pairing of CAG-CAG triads, with central A-A mismatches being flanked by two G-C base pairs (**Fig. 1a**). Thus, ligands that bind to the CAG-CAG triad also are expected to bind to the hairpin form of the $(CAG)_n$ repeat.

We previously discovered a naphthyridine-azaquinoline ligand (NA, **1**), which binds with high affinity to the CAG-CAG triad, during our investigations of small-molecular ligands that bind to base mismatches[12–15] as molecular elements for single-nucleotide polymorphism sensors[16,17] (**Fig. 1b**). The two heterocycles of NA, 2-amino-1,8-naphthyridine and 8-azaquinolone, present hydrogen bonding surfaces fully complementary to those of guanine and adenine, respectively. We assessed the binding of NA to CAG repeats through UV thermal denaturation studies. The thermal stability of a 11-mer duplex, 5′-d(CTAACAGAATG)-3′/5′-d(CATTCAGTTAG)-3′ (CAG-CAG), that contained a central CAG-CAG triad was enhanced by 34.8 °C in the presence of the NA ligand. NA-binding was highly sensitive to the identity of the base pairs flanking the central A-A mismatch (**Fig. 1c**). Qualitative analysis of the ΔT_m values suggested that NA binding involved interactions not only with the mismatched A-A pair but also with the 3′ G residue.

The stoichiometry of NA binding to the CAG-CAG triad was determined by electrospray ionization time-of-flight mass spectrometry (ESI-TOF MS) and isothermal titration calorimetry (ITC). Under ESI-MS conditions (**Fig. 1d**), CAG-CAG showed 4^- and 5^- ions of the duplex at *m/z* values of 1,668.78 and 1,334.70, respectively. Upon binding of NA to CAG-CAG, new ions appeared at *m/z* of 1,898.19 and 1,518.65, which correspond to the 4^- and 5^- ions of a complex consisting of two NA molecules and CAG-CAG. Complexes with other binding stoichiometry were not observed, even at higher NA concentrations. The association constant (K_a) of each NA molecule for the CAG-CAG triad was determined by ITC as $1.8 \times 10^6\ M^{-1}$ (**Fig. 1e**). The titration curve of the heat produced versus the DNA/ligand ratio supported a binding model involving a single set of identical sites, suggesting that two equivalent molecules of NA bind to and stabilize the CAG-CAG triad.

We carried out NMR spectroscopic structure determination to understand further how NA recognizes the CAG-CAG triad. We monitored the formation of a complex of the 11-mer duplex CAG-CAG and NA by observing shifts in one-dimensional ^1H imino proton resonances as increasing concentrations of NA were added. The imino proton chemical shifts of the NA-CAG-CAG complexes were completely different from those of the free DNA duplex. The existence of such large differences indicated that NA may intercalate into the DNA duplex[18]. Signals from free CAG-CAG and the NA-CAG-CAG complex were observed separately on a slow-exchange timescale. The stoichiometry was unambiguously determined to be 1:2 (DNA:NA), and no intermediate state was observed (**Fig. 2a** and **Supplementary Fig. 1** online). DNA signals were assigned by conventional procedures[19,20] using both unlabeled and $^{13}C^{15}N$-labeled DNA. NA signals were assigned by nuclear Overhauser effect spectroscopy (NOESY) and total correlation spectroscopy (TOCSY). Hydrogen bonding between NA and CAG-CAG was determined by analyzing the imino proton region (10–15 ppm) of NOESY (**Supplementary Fig. 2** online) and confirmed by a ^1H-^{15}N heteronuclear single-quantum coherence (HSQC) spectrum of $^{13}C^{15}N$-labeled CAG-CAG complexed with unlabeled NA (**Fig. 2b**). The solution structures of NA-CAG-CAG complexes were determined using 602 distance and dihedral constraints including 67 NA-DNA intermolecular distances (**Supplementary Fig. 3** online). Calculations of the final structure converged well, and the root-mean-square (r.m.s.) distance values were 0.79 Å for all heavy atoms of all residues, and as small as 0.54 Å for those in a well-converged region that includes A6, G7, A17, G18, NA1 and NA2

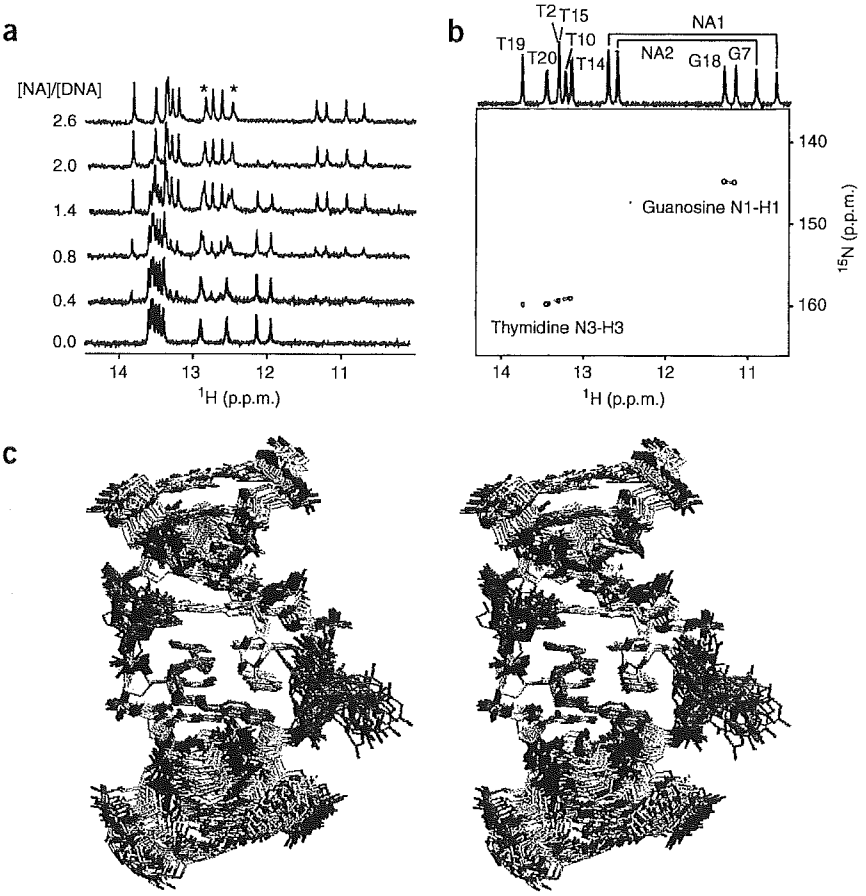

Figure 2 NMR structural analysis of NA-CAG-CAG complex. (**a**) One-dimensional ^1H spectra of 0.1 mM unlabeled 11-mer CAG-CAG at different NA concentrations at 275 K. The concentration ratios of NA to DNA are shown at left. The peaks marked with asterisks could not be observed at 293 K, the temperature at which the two-dimensional experiments were carried out. (**b**) A one-dimensional ^1H spectrum of 0.1 mM unlabeled 2:1 NA-CAG-CAG complex (top) and a ^1H-^{15}N HSQC spectrum of 0.2 mM $^{13}C^{15}N$-labeled DNA bound with the unlabeled NA (2:1 NA-CAG-CAG complex) (bottom) at 293 K. (**c**) NMR structures of NA-CAG-CAG complex. DNA is colored white, blue, red or gray except for the phosphate group, which is colored orange and red. Two NA molecules are colored yellow and orange. 30 complex structures are superimposed, focusing on A6, G7, A17, G18, NA1 and NA2 residues.

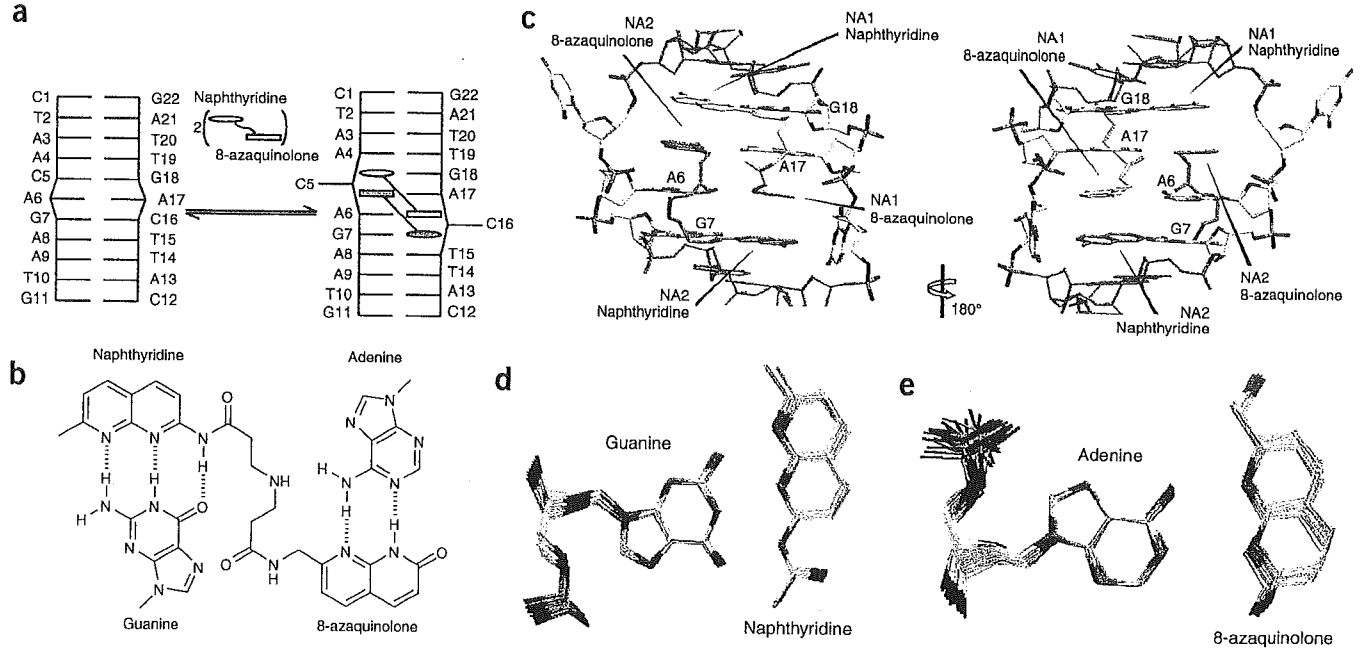

Figure 3 NA-CAG-CAG complex. (**a**) Schematic representation of the DNA conformation change induced by the complex formation, showing the free DNA (left) and NA-DNA complex (right). The face-to-face and overriding crossbars denote base pairing and base stacking, respectively. The bars sticking out to the sides, C5 and C16 of the NA-DNA complex, are the flipped-out bases. (**b**) Naphthyridine chromophore is complementary in hydrogen bonding surface to guanine, whereas 8-azaquinolone is complementary to adenine. (**c**) Major- and minor-groove views (left and right, respectively) of the NA-DNA complex structure. Two NA molecules are colored yellow (NA1) and orange (NA2), respectively. The focused and named DNA residues and NA molecules form intermolecular hydrogen bonds. (**d**) Superimposed NMR structures for the hydrogen bonding between guanine and naphthyridine. (**e**) Adenine and 8-azaquinolone.

(**Fig. 2c**). Structural and refinement statistics can be found in **Supplementary Tables 1** and **2** online.

The solution structures of the NA-CAG-CAG complex reveal how two NA molecules bind to one A-A mismatch and the 3′-G in CAG-CAG. NMR analyses showed that free CAG-CAG has a canonical B-type DNA conformation and the mismatched adenosine bases are stacked in the helix (**Fig. 3a**). In the NA-CAG-CAG complex, two mismatched adenosine bases form intermolecular hydrogen bonds with the 8-azaquinolone units of two NA molecules (**Fig. 3b**). The most unusual structural feature of the NA-CAG-CAG complex is the invasion of the G-C base pair by naphthyridine moieties. Thus, A6 and G18 bases were bound to the 8-azaquinolone and naphthyridine chromophores of NA1, respectively (**Fig. 3c**, yellow), and G7 and A16 were similarly bound to NA2 (**Fig. 3c**, orange) As a consequence, the two widowed cytidine nucleotides were extruded from the π-stack and produced two C-bulge loops. Base flipping has been observed in the complex between DNA and repair proteins[21]. The NA-CAG-CAG structure determined by NMR is notable because invasion of a small-molecule naphthyridine chromophore in NA forced the cytosine to flip out of the helix. We believe this is the first observation of induction of nucleotide flipping by a small-molecular ligand.

Naphthyridine-guanine and 8-azaquinolone–adenine pairs are well stacked in the right-handed DNA helix, showing structural mimicry of Watson-Crick base pairing (**Fig. 3d,e**). The structural studies indicated that each NA binds to an adenine base on one strand and a guanine base on the opposite strand. Neither the NMR data nor the UV melting experiment supports the possibility of an alternative intrastrand NA-CAG-CAG complex (**Supplementary Fig. 4** online). These cross-stranded interactions may explain the notably greater stability of the NA-CAG-CAG complex, as compared to the uncomplexed DNA, observed in the UV thermal denaturation

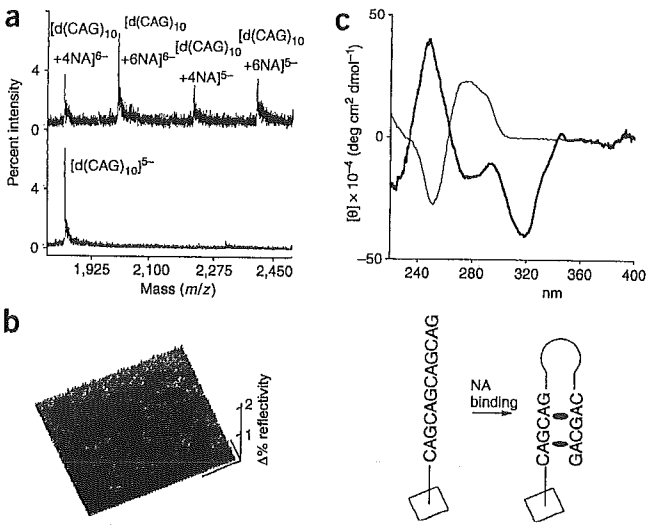

Figure 4 NA binding to the $(CAG)_n$ repeats. (**a**) ESI-TOF MS of $d(CAG)_{10}$ in the absence (below) and presence (above) of NA. (**b**) Left, SPR difference images of CAG and CTG repeats immobilized on a gold surface upon binding of NA. Key: a, HS-$d(T_{15}(CAG)_{10})$; b, HS-$d(T_{15}(CTG)_{10})$; c, blank. Right, an image of induced hairpin formation on the sensor resulting from NA binding. (**c**) CD spectral change induced on $(CAG)_{10}$ (5 μM) upon binding of NA (50 μM) with 100 mM NaCl in sodium cacodylate (pH 7.0, 10 mM). Key: $(CAG)_{10}$, thin line; $(CAG)_{10}$ + NA, bold line.

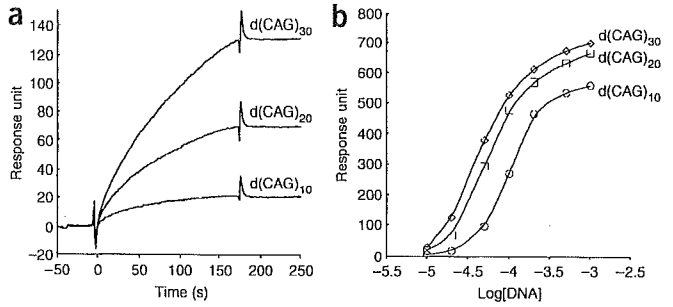

Figure 5 SPR analyses of the $(CAG)_n$ repeats by NA-immobilized sensor surface. (**a**) Binding of $d(CAG)_{10}$, $d(CAG)_{20}$ and $d(CAG)_{30}$ (each 20 nM) was measured in HEPES buffer (pH 7.4) containing 150 mM NaCl with the sensor surface where a dimeric form of NA was immobilized for 364 response units. (**b**) Dynamic range of NA-immobilized SPR sensor for the $(CAG)_n$ repeats detection. The signal intensity at 200 s of analysis was plotted. DNA concentrations were 10, 20, 50, 100, 200, 500 and 1,000 nM.

studies. These structural features also are consistent with ITC results indicating that the NA-CAG-CAG complex is stabilized by a large negative ΔH term (–16.2 kcal mol^{-1}), compensating for a negative ΔS term (–28.8 cal mol^{-1} K^{-1}).

Strong NA binding to the CAG-CAG triad induced formation of the NA-bound hairpin form in long $(CAG)_n$ repeats. ESI-TOF MS of a 30-mer single-stranded $d(CAG)_{10}$ containing ten CAG repeats in the presence of NA showed a series of ions corresponding to NA adducts of (4NA + $d(CAG)_{10}$) and (6NA + $d(CAG)_{10}$) (**Fig. 4a**). Each of these ions contained an even number of NA molecules, supporting the idea that the binding of NA to the $(CAG)_n$ repeat proceeds in a pairwise combination, as we demonstrated for the NA-CAG-CAG complex. To determine whether any conformational change is induced in the $(CAG)_n$ repeat upon binding of NA, we monitored surface plasmon resonance (SPR) difference images[22,23] of a gold surface modified with oligomers containing $d(CAG)_{10}$ and $d(CTG)_{10}$ (**Fig. 4b**). Upon exposure of this surface to an NA solution, SPR difference images were observed selectively at sites of $d(CAG)_{10}$ but not $d(CTG)_{10}$ immobilization. The reflectivity change in SPR at $d(CAG)_{10}$ spots upon NA binding was larger than that produced by hybridization with $d(CTG)_{10}$ (data not shown). Circular dichroism spectra of $d(CAG)_{10}$ also showed a large conformational change upon NA binding (**Fig. 4c**). Measurements of UV melting, ESI-TOF and fluorescence resonance energy transfer (FRET) labeling with the fluorophores 6-FAM and TAMRA at the 5′ and 3′ ends, respectively, also supported hairpin formation by $(CAG)_n$ (**Supplementary Fig. 5** online).

Given the ability of NA to bind CAG repeats, we created a sensor in which NA was immobilized on an SPR chip and assessed its utility for diagnosis of the CAG repeat length by SPR analysis. Because of the pairwise binding mechanism, we immobilized NA in dimeric form on the sensor surface (**Supplementary Methods** online). SPR analyses of the binding of $d(CAG)_{10}$, $d(CAG)_{20}$ and $d(CAG)_{30}$ to the immobilized NA dimer showed that signal intensities increased with repeat length (**Fig. 5a**). The SPR intensities of $d(CAG)_{30}$ were stronger than those of $d(CAG)_{10}$ and $d(CAG)_{20}$ at a wide range of DNA concentrations (**Fig. 5b**), suggesting that it may be possible to use the dimeric NA-immobilized SPR sensor for the rapid diagnosis of CAG repeat length.

Currently, there is no effective therapeutic agent for treating diseases caused by triplet repeat expansion. Recently, DNA alkylating agents have been shown to greatly reduce the $(CTG)_n$ repeat length in lymphoblast cells[24]. The discovery of the small-molecular ligand NA, which binds with high affinity to repeat sites, may be a substantial step toward developing effective therapeutic agents for these hereditary diseases.

METHODS

Materials. The ligand NA was synthesized as we have described[14]. All commercially available buffers and other chemicals were of the highest quality available. The oligonucleotides were purchased from Fasmac.

Melting temperature measurements. Melting temperatures of duplexes containing A-A mismatches (5 μM each strand) were recorded on a Shimadzu UV-2550 spectrophotometer with the TMSPC-8 analysis system in the absence and presence of NA (200 μM) in 10 mM sodium cacodylate buffer (pH 7.0) and 100 mM NaCl. ΔT_m is calculated as the difference of T_m in the presence and the absence of NA.

ESI-TOF MS measurements. Samples were prepared by mixing DNA (20 μM) and NA (120 μM) in 45–50% methanol in water containing 100 mM ammonium acetate. Mass spectra were obtained with an Applied Biosystems Mariner mass spectrometer and JEOL AccuTOF JMS-T100N mass spectrometer.

ITC measurements. A solution of CAG-CAG (10 μM) was titrated with NA solution (200 μM) at 5 °C in 10 mM sodium cacodylate buffer (pH 7.0) and 100 mM NaCl on a MicroCal VP-ITC calorimeter. Thermodynamic parameters were calculated from the binding curve using analytical software supplied with the instrument with a binding model involving a single set of identical sites.

NMR experiments. All data were collected on Bruker AVANCE500 and DRX800 NMR spectrometers. Titration experiments were carried out at 275 K using 0.1 and 0.8 mM unlabeled DNA duplex. Water-flipback NOESY spectra with mixing times of 30, 100, 150 and 200 ms were recorded at 293 and 303 K in H_2O or D_2O using the 0.8 mM unlabeled sample. TOCSY and double-quantum filtered correlation spectroscopy (DQF-COSY) spectra were recorded under similar conditions. ^1H-^{15}N HSQC, ^1H-^{13}C HSQC, and three-dimensional HCCH-TOCSY spectra were observed at 293 K in H_2O using a 0.2 mM uniformly $^{13}C^{15}N$-labeled sample. The labeled sample was prepared using a primer extension method[25]. All samples were dialyzed against a 50 mM sodium phosphate buffer (pH 6.5), 100 mM NaCl and 0.1 mM EDTA before measurements.

Structure determination. Interproton distance bounds were determined from the integrated peak intensities by the random error MARDIGRAS (RAND MARDI) procedure of the complete relaxation matrix analysis method[26]. Based on DQF-COSY, NOESY and phosphorus spectra, sugar puckers and backbone torsion angles were restrained to maintain an S-type sugar conformation and right-handed helix, respectively. Hydrogen-bonding restraints were imposed on the Watson-Crick base pairs and the NA-DNA hydrogen-bonding pairs. 422 distance constraints, including 58 sequential and 67 intermolecular distances and 180 dihedral angle constraints, were collected. The complex structure was calculated with a simulated annealing protocol using Crystallography & NMR System (CNS)[27]. Thirty structures without a distance violation greater than 0.5 Å were selected.

SPR imaging measurements. 5′-Thiol-modified oligomers HS-$d(T_{15}(CAG)_{10})$ and HS-$d(T_{15}(CTG)_{10})$, containing a dT_{15} spacer, were immobilized on the gold surface through the use of a hydrophilic heterobifunctional cross-linker[28]. The surface was exposed to NA (1 mM) for 200 s and then to buffer (10 mM phosphate, 300 mM NaCl, pH 7.4) in the SPR imaging instrument (Multi-SPRinter, Toyobo). The immobilized sites of the CAG and CTG repeats were confirmed by hybridization with corresponding complementary strands. The image was obtained by subtracting the data before and after interaction with NA.

SPR analyses for $(CAG)_n$ repeat number. A dimeric form of NA was synthesized by coupling of two molecules of NA and *N*-Boc imino-3,3′-bis(pentafluorophenylpropionate). After deprotection of the Boc group, the resulting secondary nitrogen was coupled with 4-*N*-Boc-amino-*N*-(3-oxopropyl)-butyramide. The terminal Boc group was removed to generate a

primary amine for the immobilization to the surface. A standard method recommended by Biacore was used for the immobilization to the carboxymethyl dextran surface of CM-5 sensor (Biacore). The amount of immobilized ligand was determined by the difference of SPR intensity before and after ligand immobilization. The SPR sensorgrams were obtained with a Biacore 2000 instrument (Biacore).

Accession codes. Atomic coordinates have been deposited in the Protein Data Bank under accession number 1X26.

Note: Supplementary information is available on the Nature Chemical Biology website.

ACKNOWLEDGMENTS

We thank T.L. James and M. Shimizu for valuable discussions. This work was partially supported by a Grant in Aid for Scientific Research (A) from the Japan Society for the Promotion of Science to K.N., Health and Labour Sciences Research Grants for Research on Advanced Medical Technology from the Ministry of Health, Labour and Welfare to K.N. and C.K., and CREST, Japan Science and Technology Agency to K.N.

COMPETING INTERESTS STATEMENT

The authors declare that they have no competing financial interests.

Received 7 January; accepted 21 April 2005
Published online at http://www.nature.com/nchembio/

1. Ashley, C.T. & Warren, S.T. Trinucleotide repeat expansion and human disease. *Annu. Rev. Genet.* **29**, 703–728 (1995).
2. Paulson, H.L. & Fishbeck, K.H. Trinucleotide repeats in neurogenetic disorders. *Annu. Rev. Neurosci.* **19**, 79–107 (1996).
3. Wells, R.D. & Warren, S.T. (eds). (1998) *Genetic Instabilities and Hereditary Neurological Diseases.* Academic Press, San Diego.
4. McMurray, C.T. DNA secondary structure: A common and causative factor for expansion in human disease. *Proc. Natl. Acad. Sci. USA* **96**, 1823–1825 (1999).
5. Duyao, M.P. *et al.* Trinucleotide repeat length: instability and age of onset in Huntington's disease. *Nat. Genet.* **4**, 387–392 (1993).
6. Mangiarini, L. *et al.* Instability of highly expanded CAG repeats in mice transgenic for the Huntington's disease mutation. *Nat. Genet.* **15**, 197–200 (1997).
7. Gacy, A.M., Goellner, G., Juranic, N., Macura, S. & McMurray, C.T. Trinucleotide repeats that expand in human disease form hairpin structures in vitro. *Cell* **81**, 533–540 (1995).
8. Mitas, M. *et al.* Hairpin properties of single-stranded-DNA containing a GC-rich triplet repeat: $(CTG)_{15}$. *Nucleic Acids Res.* **23**, 1050–1059 (1995).
9. Petruska, J., Arnheim, N. & Goodman, M.F. Stability of intrastrand hairpin structures formed by the CAG/CTG class of DNA triplet repeats associated with neurological diseases. *Nucleic Acids Res.* **24**, 1992–1998 (1996).
10. Ohshima, K. & Wells, R.D. Hairpin formation during DNA synthesis primer realignment in vitro triplet repeat sequences from human hereditary disease genes. *J. Biol. Chem.* **272**, 16798–16806 (1997).
11. Freudenreich, C.H., Stavenhagen, J.B. & Zakian, V.A. Stability of a CTG/CAG trinucleotide repeat in yeast is dependent on its orientation in the genome. *Mol. Cell. Biol.* **17**, 2090–2098 (1997).
12. Nakatani, K., Sando, S. & Saito, I. Scanning of guanine-guanine mismatches in DNA by synthetic ligands using surface plasmon resonance. *Nat. Biotechnol.* **19**, 51–55 (2001).
13. Nakatani, K., Sando, S., Kumasawa, H., Kikuchi, J. & Saito, I. Recognition of guanine-guanine mismatches by the dimeric form of 2-amino-1,8-naphthyridine. *J. Am. Chem. Soc.* **123**, 12650–12657 (2001).
14. Hagihara, S. *et al.* Detection of guanine-adenine mismatches by surface plasmon resonance sensor carrying naphthyridine-azaquinolone hybrid on the surface. *Nucleic Acids Res.* **32**, 278–286 (2004).
15. Kobori, A., Horie, S., Suda, H., Saito, I. & Nakatani, K. The SPR sensor detecting cytosine-cytosine mismatches. *J. Am. Chem. Soc.* **126**, 557–562 (2004).
16. Syvänen, A-C. Accessing genetic variation: genotyping single nucleotide polymorphisms. *Nat. Rev. Genet.* **2**, 930–942 (2001).
17. Nakatani, K. Chemistry challenge in SNP typing. *ChemBioChem* **5**, 1623–1633 (2004).
18. Han, X. & Gao, X. Sequence specific recognition of ligand-DNA complexes studied by NMR. *Curr. Med. Chem.* **8**, 551–581 (2001).
19. Wuthrich, K. NMR of proteins and nucleic acids. (John Wiley & Sons, Inc., New York, 1986).
20. Wijmenga, S.S. & van Buuren, B.N. The use of NMR methods for conformational studies of nucleic acids. *Prog. Nucl. Magn. Reson. Spectrosc.* **32**, 287–387 (1998).
21. Roberts, R.J. & Cheng, X. Base flipping. *Annu. Rev. Biochem.* **67**, 181–198 (1998).
22. Brockman, J.M., Nelson, B.P. & Corn, R.M. Surface plasmon resonance imaging measurements of ultrathin organic films. *Annu. Rev. Phys. Chem.* **51**, 41–63 (2000).
23. Smith, E.A. *et al.* Chemically induced hairpin formation in DNA monolayers. *J. Am. Chem. Soc.* **124**, 6810–6811 (2002).
24. Hashem, V.I. *et al.* Chemotherapeutic deletion of CTG repeats in lymphoblast cells from DM1 patients. *Nucleic Acids Res.* **32**, 6334–6346 (2004).
25. Zimmer, D.P. & Crothers, D.M. NMR of enzymatically synthesized uniformly $^{13}C^{15}N$-labeled DNA oligonucleotides. *Proc. Natl. Acad. Sci. USA* **92**, 3091–3095 (1995).
26. Liu, H., Spielmann, H.P., Ulyanov, N.B., Wemmer, D.E. & James, T.L. Interproton distance bounds from 2D NOE intensities: effect of experimental noise and peak integration errors. *J. Biomol. NMR* **6**, 390–402 (1995).
27. Brunger, A.T. *et al.* Crystallography & NMR system: A new software suite for macromolecular structure determination. *Acta Crystallogr. D* **54**, 905–921 (1998).
28. Kyo, M. *et al.* Evaluation of MafG interaction with Maf recognition element arrays by surface plasmon resonance imaging technique. *Genes Cells* **9**, 153–164 (2004).

Available online at www.sciencedirect.com
SCIENCE DIRECT®
Bioorganic & Medicinal Chemistry
ELSEVIER
Bioorganic & Medicinal Chemistry 13 (2005) 4507–4512

N,N'-Bis(3-aminopropyl)-2,7-diamino-1,8-naphthyridine stabilized a single pyrimidine bulge in duplex DNA

Hitoshi Suda, Akio Kobori, Jinhua Zhang, Gosuke Hayashi and Kazuhiko Nakatani*

Department of Synthetic Chemistry and Biological Chemistry, Faculty of Engineering, Kyoto University, Kyoto 615-8510, Japan

Received 2 March 2005; revised 15 April 2005; accepted 15 April 2005
Available online 23 May 2005

Abstract—We here show the first identified ligand 2,7-diamino-1,8-naphthyridine (DANP) that strongly and specifically binds to the single cytosine and thymine bulges with exclusively 1:1 stoichiometry.

Small molecules that bind to bulges and mismatches in duplex DNA and those covalently attached to DNA are important probes for the dynamics of unusual DNA structures.[1,2] With a combination of bulge- and mismatch-forming hybridization, these molecules are also useful for the detection of base mutation and deletion.[3,4] Toward this end, we have investigated a series of compounds that have hydrogen-bonding surface fully complementary to that of the unpaired or partially paired nucleotide bases, and found that 2-amino-1,8-naphthyridine and 8-azaquinolone effectively functioned as a molecular element for the recognition of guanine and adenine bases, respectively.[5,6] For the cytosine, Teramae and co-workers used 2-amino-1,8-naphthyridine and proposed formation of two hydrogen bonds to the cytosine.[7] We have independently reported that a dimeric form of 2-amino-1,8-naphthyridine strongly stabilized C–C mismatches.[8] Because these ligands bound to the bulge and mismatched structure in duplex DNA, the equilibrium between single strands and a duplex shifted toward the duplex state, making the apparent stability of the duplex increase. In the study, we proposed a formation of three hydrogen bonds between a protonated form of 2-amino-1,8-naphthyridine and the cytosine. As protonation of the nitrogen in the heterocycles effectively modulated the hydrogen-bonding surface of the molecule, further studies were carried out to see the scope and limitation of the idea. We here describe a new molecular probe *N,N'*-bis(3-aminopropyl)-2,7-diamino-1,8-naphthyridine (DANP) that could stabilize not only a single cytosine but also the thymine bulge in duplex DNA (Chart 1). Cold spray ionization time-of-flight mass spectrometry showed that DANP bound to the cytosine and thymine bulges with a 1:1 stoichiometry. The pH dependency of UV spectra of 2,7-diamino-1,8-naphthyridine supported the hydrogen bonding of DANP to the cytosine and thymine through the protonated form.

We have focused on the 2,7-diamino-1,8-naphthyridine, because it has an alignment of hydrogen-bonding groups in the order of a donor (D), acceptor (A), acceptor, and donor. We anticipated that rich hydrogen-bonding groups in one edge of a planar aromatic ring provide a good chance to form stable complex with bulged nucleotides in duplex DNA. DANP was obtained by nucleophilic substitution of 2,7-dichloro-1,8-naphthyridine[9] with 1,3-propandiamine (Scheme 1). Since the initially formed DANP was difficult to isolate from 1,3-propandiamine used as a solvent, the crude

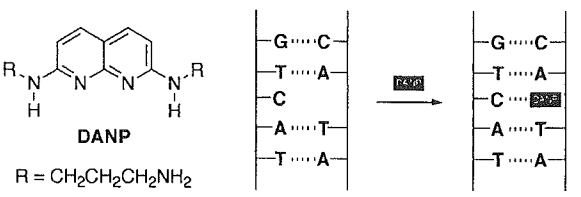

Chart 1. Structure of DANP and an illustration of DANP mediated stabilization of C-bulge.

Keywords: Cytosine; Bulge; CSI-TOF; DNA.
* Corresponding author at present address: Department of Regulatory Bioorganic Chemistry, The Institute of Scientific and Industrial Research, Osaka University, Ibaraki 567-0047, Japan. Tel.: +81 668 798 455; fax: +81 668 798 459; e-mail: nakatani@sanken.osaka-u.ac.jp

0968-0896/$ - see front matter © 2005 Elsevier Ltd. All rights reserved.
doi:10.1016/j.bmc.2005.04.035

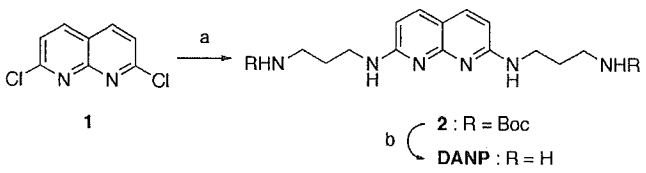

Scheme 1. Reagents and conditions: (a) 1,3-diaminopropane, 60 °C, 24 h, then $(Boc)_2O$, $CHCl_3$, 53%; (b) HCl, EtOAc, $CHCl_3$, quantitative.

product was treated with di-*tert*-butyl dicarbonate to produce Boc-protected DANP. After purification by silica gel column chromatography, the Boc protecting group was removed to give DANP.

The binding of DANP to DNA containing a single nucleotide bulge was examined by measuring melting temperature (T_m) of duplexes 5′-d(TCCAX_YCAAC)-3′/3′-d(AGGTZNWGTTG)-5′ containing a single nucleotide bulge **N**, where **N** was adenine, guanine, cytosine, or thymine. The **X**–**Z** and **Y**–**W** were any combinations of Watson–Crick base pairs. Duplexes containing the cytosine bulge in all 16 flanking sequences [4(**X**–**Z**) × 4(**Y**–**W**)] were significantly stabilized as judged by the increase of T_m (ΔT_m) in the presence of DANP (100 μM) (ΔT_m = 7.0–12.4 °C) (Fig. 1). The largest ΔT_m (12.4 ° C) was recorded for the duplex 5′-d(TCCA-T_ACAAC)-3′/3′-d(AGGTACTGTTG)-5′ (**T_A/ACT**) where the cytosine bulge was flanked by T–A and A–T base pairs. It was also shown that thymine bulges were effectively stabilized by DANP binding (ΔT_m = 4.7–9.4 °C). In contrast, the T_m increases of guanine (ΔT_m = 3.2–5.6 °C) and adenine (ΔT_m = 2.3–5.7 °C) bulges were less significant as compared to that observed for the cytosine and thymine bulges. It is noteworthy that fully matched duplexes 5′-d(TCCAXYCAAC)-3′/3′-d(AGGTZWGTTG)-5′, where **X**–**Z** and **Y**–**W** were any combinations of Watson–Crick base pairs were only weakly stabilized (ΔT_m = 0.5–2.0 °C) under the set conditions (data not shown). These results indicated that DANP showed a preference for the binding to the single pyrimidine bulge over the purine bulge and fully matched duplexes.

The stoichiometry for the binding of DANP to the cytosine and thymine bulge was examined by cold spray ionization time-of-flight mass spectrometry (CSI-TOF MS).[10] In the presence of two molar equivalents of DANP to the cytosine bulge duplex **T_A/ACT**, a distinct ion at *m/z* of 1323.81 and 1654.96 corresponding to 5^- and 4^- ion, respectively, of a 1:1 complex was detected in addition to the intact duplex (Fig. 2). Further increase of the DANP concentration to 6 equiv resulted in an increase of the ion intensity of the 1:1 complex with a concomitant decrease of the intact duplex. Under the conditions, complexes with other binding stoichiometries could not be detected. Similarly, CSI-TOF MS showed a 1:1 complex between DANP and the thymine bulge duplex 5′-d(TCCAT_ACAAC)-3′/3′-d(AGG-TATTGTTG)-5′ (**T_A/ATT**) (Fig. 3). With increasing the amount of DANP, the ion corresponding to the 1:1 complex (*m/z* 1326.42) increased with a concomitant decrease of the ion corresponding to the intact duplex

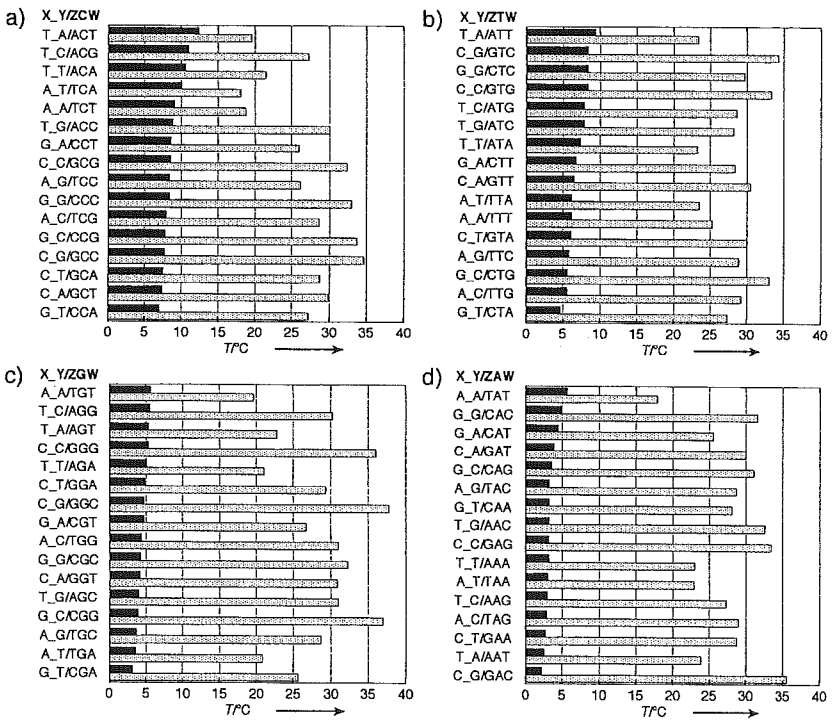

Figure 1. Effects of DANP-binding on the melting temperatures of 5′-d(TCCAX_YCAAC)-3′/3′-d(AGGTZNWGTTG)-5′ containing a single nucleotide bulge (**N**) flanked by **X**–**Z** and **Y**–**W** base pairs. Melting temperature (T_m) of duplex (4.8 μM) measured in sodium cacodylate buffer (pH 7.0, 10 mM) and sodium chloride (100 mM) was shown with a gray bar. Increase of T_m (ΔT_m) in the presence of DANP (100 μM) was shown with a black bar. The flanking base pairs (**X**–**Z** and **Y**–**W**) were shown in the left of the bar. Key: (a) C bulge (N = C), (b) T bulge (N = T), (c) G bulge (N = G), and (d) A bulge (N = A).

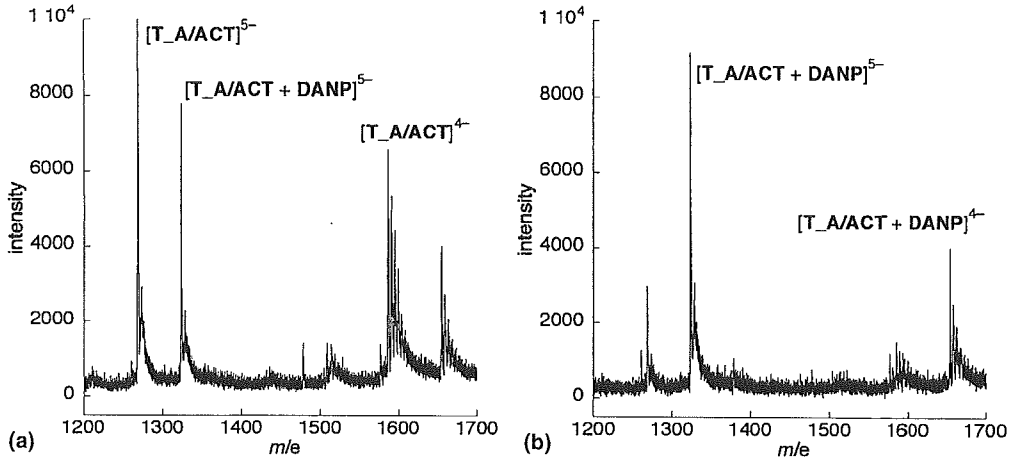

Figure 2. CSI-TOF MS of 5′-d(TCCAT_ACAAC)-3′/3′-d(AGGTACTGTTG)-5′ (T_A/ACT) (20 μM) measured in 50% aqueous methanol and 100 mM ammonium acetate in the presence of (a) 40 and (b) 120 μM of DANP.

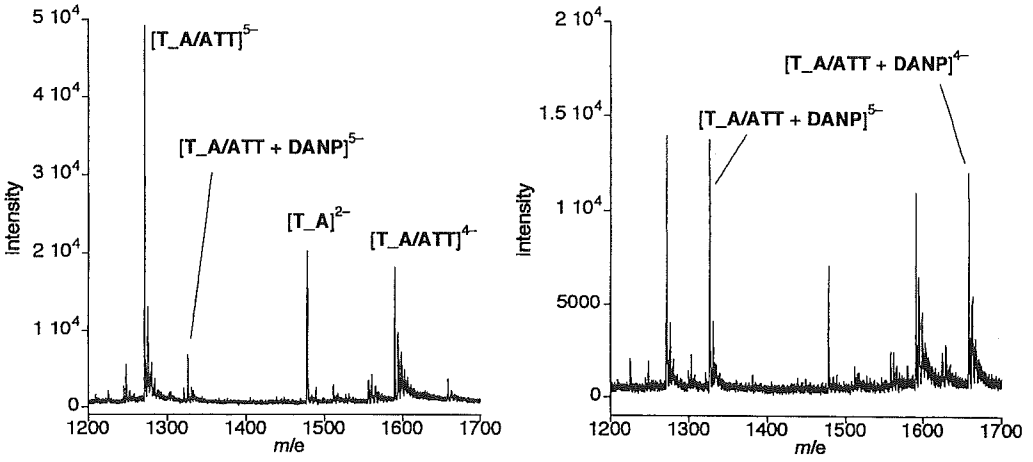

Figure 3. CSI-TOF MS of 5′-d(TCCAT_ACAAC)-3′/3′-d(AGGTATTGTTG)-5′ (T_A/ATT) (20 μM) measured in 50% aqueous methanol and 100 mM ammonium acetate in the presence of (a) 40 and (b) 120 μM of DANP.

(*m/z* 1271.57). These CSI-TOF MS experiments strongly suggested that DANP bound to both cytosine and thymine bulge with a 1:1 stoichiometry. In the presence of 6 equiv of DANP, the ion intensity corresponding to the intact duplex was much higher for the thymine bulge than for the cytosine bulge, suggesting that DANP binding to the cytosine bulge would be stronger than to the thymine bulge. This is consistent with a larger ΔT_m observed for the cytosine bulge than for the thymine bulge in the same T_A/ANT (N = C or T) sequence context. The association constant for the DANP binding to the cytosine bulge was determined to be $7.5 \times 10^5\ M^{-1}$ by fluorescence titration and Scatchard plot analysis (data not shown).

To gain further insight into the DANP binding to the cytosine and thymine bulges, the pH dependency of DANP absorption spectra were examined. Absorption spectra of DANP free in solution were sensitive to the pH of the solution (Fig. 4a). At pH 8.5, the absorption maximum was observed at 365 nm, whereas it shifted to 376 nm at pH 5.0. A plot of the absorbance at 376 nm against the solution pH showed a sigmoid curve (Fig. 4b). The pH dependency of the UV absorbance of DANP was rationalized by a protonation at the nitrogen in a 2,7-diamino-1,8-naphthyridine chromophore. Energy calculation in an aqueous solvent using the Cramer–Truhlar solvation methods with density functional theory (B3LYP/6-31G(d)) indicated that a protonation at *N*1 of the 2,7-diamino-1,8-naphthyridine chromophore was energetically much more favorable by 6.9 kcal/mol than a protonation at the 2-amino group. A pK_a of 6.8 for the protonated form of DANP ($DANPH^+$) was obtained as the pH at the inflection of the curve. A protonation of *N*1 of DANP resulted in the modulation of the hydrogen-bonding surface from an alignment of D–A–A–D in DANP to a D–A–D–D alignment in $DANPH^+$. The D–A–D–D alignment of the hydrogen-bonding groups in $DANPH^+$ is fully complementary not only to that of cytosine (D–A–A) but also to that of thymine base (A–D–A). The complementarily hydrogen bonding surface to that of the cytosine and thymine is most likely to rationalize the selective binding of DANP to pyrimidine bases. In a proposed hydrogen-bonding scheme between $DANPH^+$ and cytosine, the proton attached *N*1 would be bound by *N*3 of

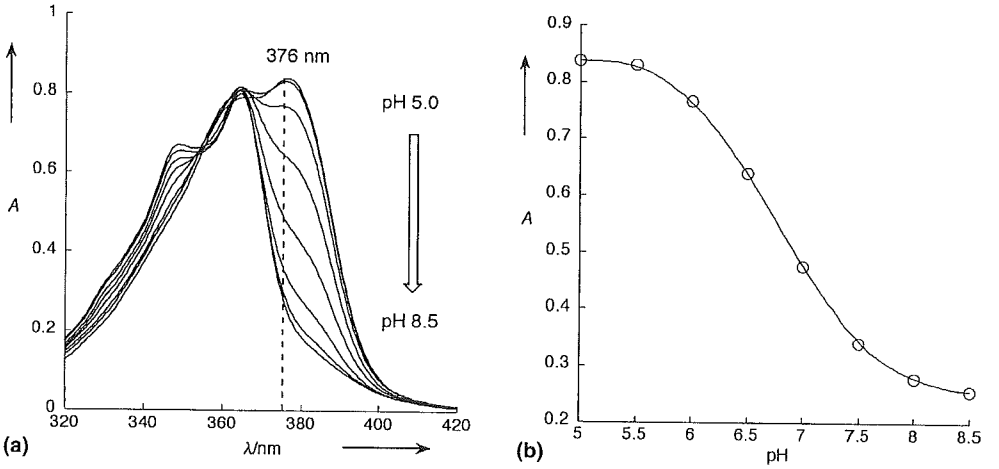

Figure 4. (a) Absorption spectra of DANP (100 μM) recorded at pH of 5.0, 5.5, 6.0, 6.5, 7.0, 7.5, 8.0, and 8.5 in sodium phosphate buffer (10 mM) and sodium chloride (100 mM). (b) A plot of absorption at 376 nm against the solution pH.

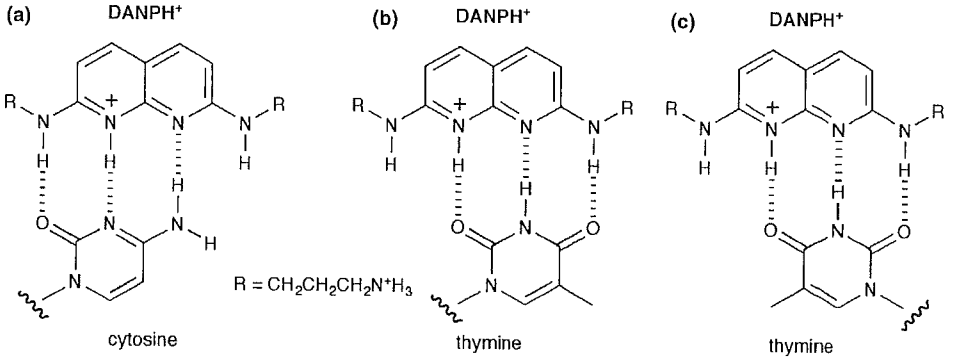

Figure 5. Proposed hydrogen-bonding schemes between $DANPH^+$ and pyrimidine nucleobases. Key: (a) cytosine, (b) and (c) thymine. Two orientations are conceivable for hydrogen bonding of $DANPH^+$ to thymine.

the cytosine. Due to a palindromic A–D–A alignment of hydrogen-bonding groups in the thymine base, two orientations were conceivable for the hydrogen bonding to $DANPH^+$. The difference in the two orientations was that the non-hydrogen bonding amino group was located either in a minor groove (Fig. 5b) or in a major groove of the $DANPH^+$–DNA complex (Fig. 5c).

When aromatic molecules intercalated into DNA, the electronic state of the molecule would be significantly affected by the stacking interaction with the neighboring base pairs. It was confirmed that DANP showed a large spectroscopic change upon binding to a single pyrimidine bulge. The UV absorption was measured with a constant DANP (10 μM) and DNA (30 μM) concentration in phosphate buffer (pH 7.0) and 100 mM NaCl. Free DANP in phosphate buffer (pH 7.0) showed absorption maximum at 364 nm with a shoulder at 376 nm. The presence of fully matched duplex as well as adenine bulge duplex resulted in a small hypochromic shift but not a bathochromic shift of the absorption maximum (Fig. 6a). In contrast, the cytosine bulge duplex (**T_A/ACT**) induced a bathochromic shift by 30 nm to 394 nm with a concomitant hypochromic shift by 65%. Bathochromic shift of DANP absorption was also induced by the thymine bulge (**T_A/ATT**) producing the absorption maximum at 390 nm. Guanine bulge duplex was intermediate between the pyrimidine and adenine bulge duplex in terms of the bathochromic shift. In response to the bathochromic shift, fluorescence spectra of DANP showed a significant change with respect to the emission wavelength and the shape of the spectra. The fluorescence spectra of DANP free in solution excited at its absorption maximum showed an emission maximum at 394 nm in pH 7.0. The emission maximum of DANP was not virtually affected by the presence of fully matched duplex and adenine bulge duplex. However, a broad emission with the emission maximum at 424 nm was observed in the presence of the cytosine bulge. In the presence of thymine bulge, a similar fluorescence spectrum was obtained with a decreased intensity. Quantum yield of DANP fluorescence at 424 nm obtained by an excitation at 394 nm in the presence of **T_A/ACT** and **T_A/ATT** were 0.332 and 0.166, respectively.

The results described here showed that DANP bound not only to the cytosine but also to the thymine bulge. The selective DANP binding to these pyrimidine bulges was most plausible by the protonation of the nitrogen in the 2,7-diamino-1,8-naphthyridine chromophore, producing hydrogen-bonding surfaces fully complementary to those of cytosine and thymine. We have demonstrated that molecules having hydrogen-bonding surface

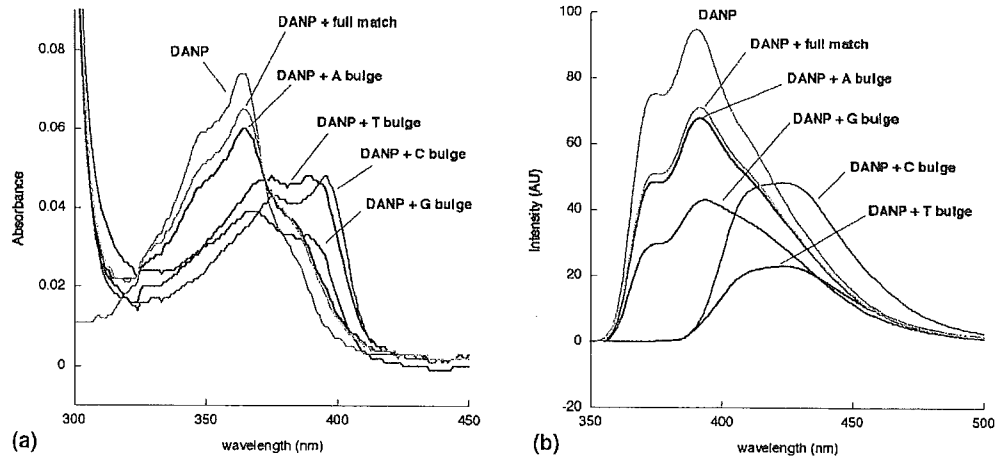

Figure 6. (a) Absorption spectra of DANP (10 μM) recorded in the presence of duplexes 5′-d(TCCAT_ACAAC)-3′/3′-d(AGGTANTGTTG)-5′ containing N bulge (N = C, T, G, and A) (30 μM) and 10-mer fully matched duplexes 5′-d(TCCATACAAC)-3′/3′-d(AGGTATGTTG)-5′ (30 μM) in sodium phosphate buffer (pH 7.0, 10 mM) and sodium chloride (100 mM). (b) Fluorescence spectra of DANP recorded under the same conditions. Excitation wavelength was at the absorption maxima.

fully complementary to the nucleotide bases were useful probes for the detection of bulges and mismatches in duplex DNA. Because, protonation of the nitrogen in heterocycles could effectively modulate the hydrogen-bonding surface from the acceptor to the donor, the idea of the protonation of the chromophore may provide a new way for the design of a molecular element for the base recognition. Furthermore, the observed spectroscopic changes upon binding of DANP to pyrimidine bulges could be applicable to the detection of the single pyrimidine bulge in duplex DNA.

1. Experimental

1.1. {3-[7-(3-{*tert*}-Butoxycarbonylamino-propylamino)-[1,8]naphthyridin-2-ylamino]-propyl}-carbamic acid *tert*-butyl ester (*2*)

A mixture of **1** (50 mg, 0.25 mmol) and 1,3-diaminopropane (2 ml, 23.9 mmol) was stirred at 60 °C for 24 h. The solvent was evaporated in vacuo. The residue was dissolved in chloroform (5 ml) and was added $(Boc)_2O$ (300 mg, 1.37 mmol). The mixture was stirred at 40 °C for 6 h. Solvents were evaporated in vacuo and the resulting solid was purified by silica gel column chromatography ($CHCl_3/CH_3OH$ and hexane/AcOEt) to give **2** (62.9 mg, 53%) as yellow solids: ^1H NMR ($CDCl_3$, 400 MHz) $\delta = 7.54$ (d, 2H, $J = 8.8$ Hz), 6.34 (d, 2H, $J = 8.8$ Hz), 3.58 (q, 4H, $J = 6.0$ Hz), 3.22 (q, 4H, $J = 6.0$ Hz), 1.78 (tt, 4H, $J = 6.0$ Hz), 1.44 (s, 18H); ^{13}C NMR ($CDCl_3$, 100 MHz) $\delta = 159.8$, 157.2, 156.6, 137.3, 110.8, 106.7, 79.3, 38.5, 37.9, 30.7, 28.5 MS (ESI), *m/e* 497 $[M+Na^+]$, 475 $[M+H^+]$; HRMS calcd for $C_{24}H_{39}NaN_6O_4$ $[M+Na^+]$ 497.2852, found 497.2834, $C_{24}H_{39}N_6O_4$ $[M+H^+]$ 475.3033, found 475.2996.

1.2. *N*,*N*′-Bis-(3-amino-propyl)-[1,8]naphthyridine-2,7-diamine (DANP)

To a $CHCl_3$ (1 ml) solution of (14.5 mg, 30.6 μmol) was added ethyl acetate containing 4 N HCl (2 ml). The mixture was stirred at room temperature for 30 min. Solvent was evaporated to dryness to give DANP (quantitative) as yellow solids: ^1H NMR (CD_3 OD, 400 MHz) $\delta = 7.79$ (d, 2H, $J = 8.8$ Hz), 6.61 (d, 2H, $J = 8.8$), 3.63 (t, 4H, $J = 6.8$ Hz), 3.42 (t, 4H, $J = 7.2$ Hz), 2.04 (tt, 4H, 7.2 Hz); ^{13}C NMR (D_2O, 100 MHz) $\delta = 157.3$, 148.5, 140.6, 109.0, 108.1, 38.6, 37.4, 26.6. MS (FAB), *m/e* 275 $[(M+H)^+]$; HRMS calcd for $C_{14}H_{23}N_6$ $[(M+'H)^+]$ 275.1984, found 275.1987.

1.3. Measurements of melting temperature of bulge-containing duplexes

DANP (100 μM) was dissolved in a sodium cacodylate (10 mM, pH 7.0) containing bulge duplex (4.8 μM) and NaCl (100 mM). The mixture was heated at 50 °C and cooled slowly to make sure that the starting oligomers is in a duplex state. The thermal denaturation profile was recorded on a SHIMADU UV2550 spectrometer equipped with a SHIMADU TMSPC-8 temperature controller. The absorbance of the sample was monitored at 260 nm from 4 to 70 °C with a heating rate of 1 °C/min.

1.4. CSI-TOF measurements

Samples were prepared by mixing DNA (20 μM) and DANP (40 and 120 μM) in 50% methanol in water containing 100 mM NH_4OAc. Mass spectra were obtained with a JEOL JMS-T100 mass spectrometer equipped with cold spray ion source. Spray temperature was set at −10 °C with a sample flow rate of 10 μL/min.

1.5. UV and fluorescent spectra measurements

UV spectra were recorded on a SHIMADU UV2550 spectrometer. Fluorescent spectra were recorded on a SHIMADU RF-5300PC. DNA samples were prepared in 10 mM sodium phosphate buffer at the designate pH in the presence of 100 mM sodium chloride. Excitation wavelength for the fluorescent measurements was the wavelength at the absorption maximum unless otherwise noted.

References and notes

1. Guest, C. R.; Hochstrasser, R. A.; Sowers, L. C.; Millar, D. P. *Biochemistry* **1991**, *30*, 3271.
2. Stivers, J. T. *Nucleic Acids Res.* **1998**, *26*, 3837.
3. Hawkins, M. E.; Balis, F. M. *Nucleic Acids Res.* **2004**, *32*, e62.
4. Nakatani, K. *ChemBioChem.* **2004**, *5*, 1623.
5. Nakatani, K.; Sando, S.; Saito, I. *Nat. Biotechnol.* **2001**, *19*, 51.
6. Hagihara, S.; Kumasawa, H.; Goto, Y.; Hayashi, G.; Kobori, A.; Saito, I.; Nakatani, K. *Nucleic Acids Res.* **2004**, *32*, 278.
7. Yoshimoto, K.; Nishizawa, S.; Minagawa, M.; Teramae, N. *J. Am. Chem. Soc.* **2003**, *125*, 8982.
8. Kobori, A.; Horie, S.; Suda, H.; Saito, I.; Nakatani, K. *J. Am. Chem. Soc.* **2004**, *126*, 557.
9. George, R. N.; Sam, J. G.; Veronica, K. M.; Frank, R. F.; Giacomo, C. *J. Org. Chem.* **1981**, *46*, 833.
10. Yamaguchi, K. *J. Mass. Spectrom.* **2003**, *38*, 473.

DNA Cleavage

DOI: 10.1002/anie.200502282

Binding of Naphthyridine Carbamate Dimer to the $(CGG)_n$ Repeat Results in the Disruption of the G–C Base Pairing

*Tao Peng and Kazuhiko Nakatani**

The expansion of the $(CGG)_n$ trinucleotide repeat in the FMR1 gene causes the neurological disorder fragile X syndrome.[1-3] The molecular basis for the $(CGG)_n$ expansion involves the formation of a metastable hairpin structure[4-6] consisting of continued 5′-CGG-3′/5′-CGG-3′ triads, in which a G–G mismatch is flanked by two G–C base pairs. We recently reported the remarkable binding of naphthyridine azaquinolone (**NA**) to the 5′-CAG-3′/5′-CAG-3′ triad in the hairpin form of the $(CAG)_n$ repeat, where the A–A mismatch was flanked by G–C base pairs. The ligand-bound structure was intriguing because 1) two **NA** molecules were bound to a single CAG/CAG triad which 2) induced the cytosine—which was hydrogen-bonded to the guanine—to flip out from the base stack (Figure 1).[7] The **NA**-immobilized sensor was useful for the rapid diagnosis of the $(CAG)_n$ repeat length. We have reported a series of ligands binding to a G–G mismatch,[8-10] and therefore the remarkable structure of **NA** bound to the CAG/CAG triad prompted us to investigate the mode of ligand binding to the CGG/CGG triad and, hence, the possibility of the cytosine flipping out in the ligand-bound complex. Herein, we report that naphthyridine carbamate dimer (**NC**)[11] binds to a single CGG/CGG triad with exclusively 2:1 **NC**/triad stoichiometry. The binding of **NC** to the CGG/CGG triad induced the disruption of the guanine–cytosine base pairing in the triad, and made the cytosine susceptible to the subsequent chemical cleavage reaction initiated by addition of hydroxylamine.

Among the ligands that we synthesized for binding to the G–G mismatch, **NC** showed a marked preference in binding to the CGG/CGG triad. The binding of **NC** to the CGG/CGG triad in the 13-mer duplex increased the melting temperature (T_m) by 23.1 °C, whereas the increase in T_m (ΔT_m) was only 6.7 °C for the GGC/GGC triad (Table 1). A survey of the effect of the flanking sequence suggested that the strong and selective **NC** binding to the CGG/CGG triad is most likely a consequence of the interaction of **NC** not only with the G–G mismatch, but also with the cytosine on the 5′ side and/or the guanine on the 3′ side.

[*] T. Peng, Prof. K. Nakatani
The Institute of Scientific and Industrial Research
Osaka University
Ibaraki 567-0047 (Japan)
Fax: (+81) 6-6879-8459
E-mail: nakatani@sanken.osaka-u.ac.jp

Supporting information for this article is available on the WWW under http://www.angewandte.org or from the author.

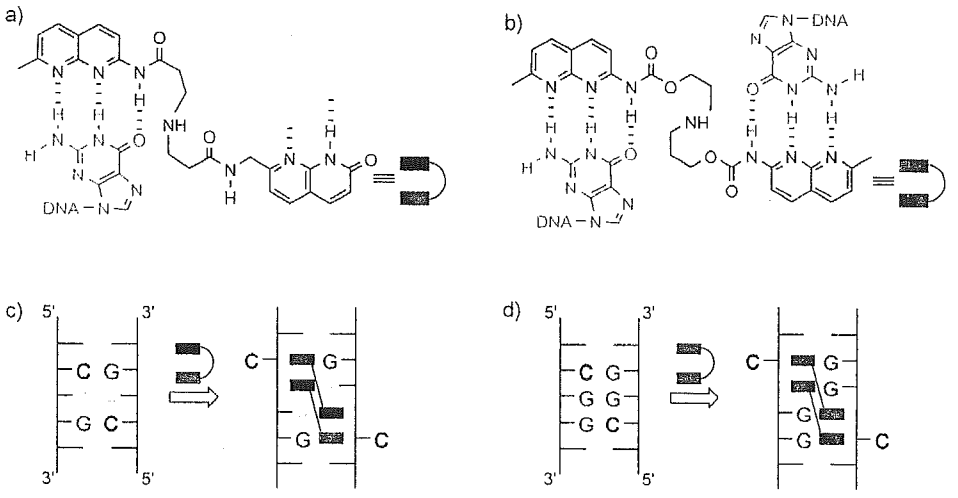

Figure 1. Hydrogen-bonding between a) **NA** and the G–A mismatch and b) **NC** and the G–G mismatch. Schematic illustrations of c) the NMR-confirmed **NA**-CAG/CAG triad complex and d) the proposed **NC** binding to the CGG/CGG triad. Red rectangles: 2-amino-1,8-naphthyridine; blue rectangles: 8-azaquinolone.

Table 1: ΔT_m [°C] and ΔT_m values [°C] for the 13-mer duplexes containing a G–G mismatch in a different flanking sequence.[a]

5'-GCTAA XGZ AATGA-3'
3'-CGATT YGW TTACT-5'

5'-XGZ-3'/5'-WGY-3'	$T_m(-)$[b]	$T_m(+)$[c]	ΔT_m[d]
CGG/CGG	34.1 (0.9)	57.2 (0.4)	23.1 (0.4)
CGC/GGG	38.6 (0.1)	49.3 (0.8)	10.7 (0.8)
GGC/GGC	40.4 (0.3)	47.1 (1.4)	6.7 (1.4)
CGA/TGG	31.8 (0.2)	44.4 (0.3)	12.6 (0.3)
CGT/AGG	33.6 (0.2)	44.0 (0.5)	10.4 (0.5)
GGA/TGC	34.2 (0.3)	43.4 (0.4)	9.2 (0.4)
AGT/AGT	28.7 (0.4)	41.9 (1.0)	13.2 (1.0)
AGG/CGT	31.8 (0.6)	39.9 (0.8)	8.1 (0.8)
GGT/AGC	33.7 (0.4)	39.3 (0.3)	5.6 (0.3)
TGA/TGA	17.8 (0.4)	35.9 (1.0)	18.1 (1.0)

[a] The UV melting curve was measured for a duplex (4.5 μM) in a sodium cacodylate buffer (10 mM, pH 7.0) containing NaCl (100 mM). The temperature was increased at a rate of 1 K min^{-1}. All measurements were made three times, and standard deviations are shown in parentheses. [b] T_m values of oligomers. [c] T_m values of oligomers in the presence of **NC** (100 μM). [d] ΔT_m was calculated as the difference between $T_m(+)$ and $T_m(-)$.

To determine the stoichiometry of the **NC**-CGG/CGG complex, cold-spray ionization time-of-flight mass spectrometry (CSI-TOF MS)[12] of the 11-mer self-complementary duplex containing the CGG/CGG triad was carried out (Figure 2). In the absence of **NC**, three ions derived from the oligomer were observed. One ion corresponded to the 3– ion of a single-stranded form ($[ss]^{3-}$; *m/z*: found 1118.13, calcd 1117.19). Duplexes were detected as a 5– ion ($[G–G]^{5-}$; *m/z*: found 1342.32, calcd 1340.83) and a 4– ion ($[G–G]^{4-}$; *m/z*: found 1678.07, calcd 1676.29). Upon addition of **NC** to the duplex with a 1:1 molar ratio, the intensity of the ions corresponding to $[ss]^{3-}$, $[G–G]^{5-}$, and $[G–G]^{4-}$ became weak, with the concomitant appearance of a new ion corresponding to the 5– ion of a 2:1 complex of **NC** and the duplex ($[G–G+2\mathbf{NC}]^{5-}$; *m/z*: found 1544.13, calcd 1542.13). A 1:1 complex was not detected. In the presence of two equivalents of **NC**, ions derived from the free duplex disappeared and only $[G–G+2\mathbf{NC}]^{5-}$ was detected. At an increased concentration of **NC**, the ion corresponding to $[G–G+2\mathbf{NC}]^{5-}$ was still predominant. These results clearly show that the binding of **NC** to the duplex containing the CGG/CGG triad proceeded exclusively with a 2:1 stoichiometry. The binding of **NC** to the CGG/CGG triad was further characterized by UV absorption titration experiments (see the Supporting Information). The crossover point of the Job's plot obtained from the titration was at 66%, which confirmed that the binding stoichiometry of **NC** to the CGG/CGG triad was 2:1, as determined by CSI-TOF MS (see the Supporting Information).

The high sequence preference and the 2:1 stoichiometry for **NC** binding are the same characteristic features that we observed for the binding of **NA** to the CAG/CAG triad.[7] Encouraged by these facts, we investigated whether the

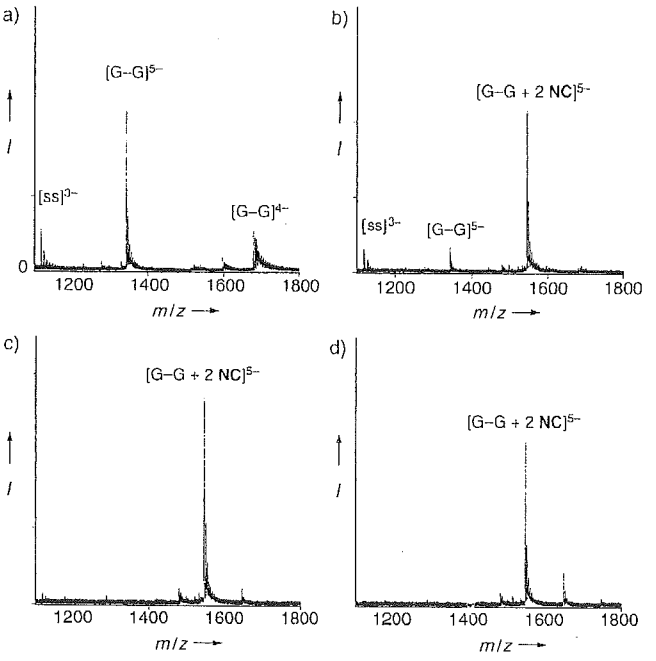

Figure 2. CSI-TOF MS of 11-mer self-complementary duplex 5'-d(TCAA CGG TTGA)-3'/5'-d(TCAA CGG TTGA)-3' containing the CGG/CGG triad. Samples contained 20 μM duplex in 50% aqueous methanol and 100 mM ammonium acetate. The sample solution was cooled at −10°C during injection at a flow rate of 0.5 mL h^{-1}. a) Duplex only; b)–d) duplex with 20, 40, and 60 μM **NC**, respectively.